Journal of Applied Physics

Shock synthesis of nanocrystalline $La_2Ti_2O_7$ powder

Cite as: J. Appl. Phys. **130**, 125903 (2021); https://doi.org/10.1063/5.0051778
Submitted: 27 March 2021 • Accepted: 01 September 2021 • Published Online: 29 September 2021

Haotian Ran, Qiang Zhou, Pengwan Chen, et al.

AIP Publishing

Journal of Applied Physics ARTICLE scitation.org/journal/jap

Shock synthesis of nanocrystalline $La_2Ti_2O_7$ powder

Cite as: J. Appl. Phys. **130**, 125903 (2021); doi: 10.1063/5.0051778
Submitted: 27 March 2021 · Accepted: 1 September 2021 ·
Published Online: 29 September 2021

Haotian Ran,[1] Qiang Zhou,[2] Pengwan Chen,[1,a)] Jianjun Liu,[3] Toshimori Sekine,[4] and Xin Gao[1,a)]

AFFILIATIONS

[1]State Key Laboratory of Explosion Science and Technology, Beijing Institute of Technology, Beijing 100081, China
[2]China Academy of Ordnance Science, Beijing 100089, China
[3]State Key Laboratory of Chemical Resource Engineering, Beijing University of Chemical Technology, Beijing 100029, China
[4]Center for High Pressure Science and Technology Advanced Research, Beijing 100094, China

[a)]**Authors to whom correspondence should be addressed:** pwchen@bit.edu.cn and gaoxin@bit.edu.cn

ABSTRACT

Perovskite $La_2Ti_2O_7$ nanocrystalline powder was obtained through the shock synthesis method. In the study, La_2O_3 and TiO_2 powders were mixed through ball milling and, subsequently, shocked by a flyer at a velocity of 3.2 km/s. After shock treatment, the sample was recovered and characterized via various techniques, such as x-ray diffraction, Raman, scanning electron microscope, transmission electron microscope, and ultraviolet-visible diffuse reflection spectrum analysis, to find the presence of $La_2Ti_2O_7$ nanocrystalline powder with an average grain size of approximately 30 nm in the recovered samples with different yields. Moreover, the results further confirm that the high shock temperature and long ball milling treatment induce higher activation of precursors to improve the $La_2Ti_2O_7$ content in the recovered samples. By adjusting the relative density of precursor and the ball milling period, pure $La_2Ti_2O_7$ nanocrystalline powder was obtained. The formation mechanism of $La_2Ti_2O_7$ was carefully illustrated. This study presents a new method to synthesize $La_2Ti_2O_7$ nanocrystalline powder by detonation-driven flyer impact.

INTRODUCTION

Metal oxides are important functional materials used in cutting-edge technology areas owing to their outstanding properties, such as thermal stability and oxidation resistance. Bimetal oxides, containing two metal elements, are important functional semiconductor materials, featuring low cost and outstanding properties beyond those of single metal oxides owing to the coupling effect of two metal elements. This type of material has been applied in various application fields, including transparent electrodes,[1] lithium-ion batteries,[2,3] dye-sensitized solar cells,[4] gas nanosensors,[5] and supercapacitors.[6] Thus, bimetal oxides have become a central focus of numerous research groups. Among them, those with the general formula of $A_2B_2O_7$ are a huge family with a vast number of element combinations. Various investigations have been reported that $A_2B_2O_7$ containing rare earth elements possess excellent properties,[7] including multiferroicity,[8] radiation resistance,[9] fluorescent center matrix materials,[10] high temperature heating elements,[11] sensors,[12,13] fuel electrode materials,[14] nuclear waste solidification,[15] and photocatalytic materials.[16] Generally, the $A_2B_2O_7$ family consists of three main crystal structures, fluorite type $A_2B_2O_7$ (e.g., $Nd_2Zr_2O_7$ and $Yb_2Zr_2O_7$), pyrochlore type $A_2B_2O_7$ (e.g., P-$Gd_2Zr_2O_7$ and $La_2Zr_2O_7$), and perovskite type $A_2B_2O_7$ [e.g., $La_2Ti_2O_7$ (LTO)].

Recently, research hubs have shown keen interest in double perovskite materials for their promising characteristics, for instance, high performance and stability in various fuels. As one typical layered double oxide with the crystalline system of $P2_1$ space group, $La_2Ti_2O_7$ (LTO) features high Curie temperature, multiferroicity, and strong photoelectric effects[17,18] and possesses excellent photocatalytic activity in the decomposition of water and pollutant degradation, and is regarded as a new generation of catalyst.[19–22]

Approaches have been reported to synthesize LTO with different properties, including conventional solid-state reaction synthesis (SSR),[21] low temperature hydrothermal synthesis,[23] the sol-gel method,[24] the liquid-feed flame spray pyrolysis (LF-FSP) method,[17] and the molten salt method.[25] In the SSR method, the mixed powder of TiO_2 and La_2O_3 was calcined at high temperature (>1000 °C) to induce a chemical reaction for the synthesis of LTO

fine powder.[21] With respect to low temperature hydrothermal synthesis, Chen and Xu[23] synthesized LTO by mixing an aqueous solution of lanthanum chloride and titanium chloride in equivalent molar proportions of La and Ti and then dropping into dilute ammonia water with stirring, the as-prepared particle size with 480 nm length and 40 nm breath. Through the sol-gel method, Prasadarao *et al.*[24] mixed $Ti(OCH(CH_3)_2)_4$, $C_6H_8O_7$, and $La(NO_3)_3{\cdot}6H_2O$ in $C_2H_6O_7$ for stirring at 60 °C to obtain a polymeric gel, then pyrolyzed to a precursor at 300–500 °C, and calcined at 500–1150 °C to obtain LTO. Abe and Laine[17] synthesized the LTO with average particle sizes of 26 nm using LF-FSP coupled through subsequent heat treatments. Huang *et al.*[25] first synthesized LTO with dandelion-like nanostructures via the molten salt method, and the dandelion structure consists of well-crystallized LTO nanorods with sizes of less than 100 nm in the radial direction and 300–500 nm in the axial direction.

Shock compression technology features high dynamic pressure, high temperature, and high quenching rate and is carried out to treat the sample with large volume compared with the static compression method. In this method, the shock wave or shock-driven flyer is utilized to act on the target material to induce ultra-high pressure and temperature in microseconds. These techniques have been widely applied in various material processing fields, such as hardening metallic material,[26,27] hybrid elements to improve the performance of composite oxides,[28,29] synthesis of novel materials,[30–32] high pressure phase material,[33,34] and activation of materials.[35] With respect to this method, several techniques have been developed to adjust the pressures and temperatures during shock compression for the synthesis of materials, such as organic molecules using inorganic precursor,[36] nanodiamond,[37–39] doped graphene,[29] and doped TiO_2.[40] The shock compression technique has been rarely reported to synthesize bimetal oxides, especially layered perovskite materials.

This study presents the synthesis of perovskite LTO nanocrystalline powder through the shock compression method using La_2O_3 and TiO_2 powders. The experimental results demonstrate that high shock temperature induced by adiabatic compression and long ball milling period are two critical factors to improve the activation of precursor for the synthesis of pure LTO through this method.

EXPERIMENTAL METHODS

For the recovery of the sample, a copper sample chamber consisting of three sample holes with a diameter of 10 mm and a height of 1 mm was applied for the shock treatment (Fig. 1). To increase the activity of the reaction, La_2O_3 (particle size 100 nm) and TiO_2 (particle size 100 nm) powders were mixed according to the mole ratio of 1:2 through ball milling treatment using a zirconia ball with a milling speed of 750 r/min in 20 g ethanol for 4 and 6 h, respectively. Then, the mixed powder used as precursor was filled into the sample holes on the sample chamber with different relative densities (ρ_{00}, identified as the ratio of precursor mass to sample hole volume). Then, the sample holes were plugged in with the copper blocks. Subsequently, a planar shock compression assembly with the chamber and the sample (Fig. 1) was set up to generate the shock wave and induce a chemical reaction. The detonation lens and main charge (8701, a mixture of RDX and polymer binder with a detonation velocity of 8315 m/s) were applied to accelerate the copper flyer. Then, the flyer impacts on the chamber to generate high temperature and high pressure in the precursor to synthesize LTO. The experimental conditions are shown in Table I.

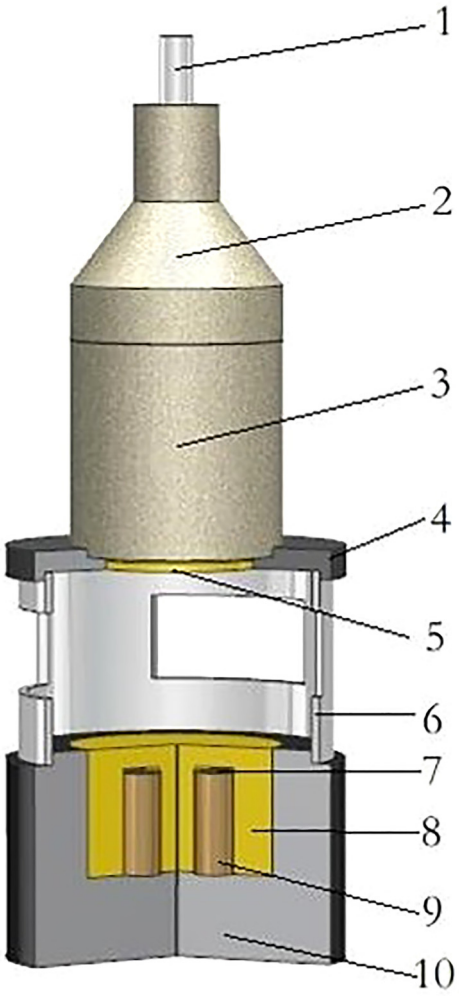

FIG. 1. Schematic of shock compression setup. 1—detonator, 2—plane wave lens, 3—8701 explosive, 4—bottom cover, 5—flyer, 6—PVC plastic tube, 7—precursor powder, 8—sample chamber with three annular evenly distributed sample holes, 9—copper lid, and 10—steel base. Note: The size of this setup is shown in the supplementary material.

During the shock process, the shock wave reflects at the upper and lower interfaces between the precursor and the container inner walls to increase the pressure and temperature of the precursor to induce the chemical reaction. After the shock experiment, the samples were recovered for further characterization. For comparison, we also prepared LTO powder using same precursor for Nos. 61–63 experiments through the SSR method at 1200 °C for 5 h.

TABLE I. Experimental conditions for shock compression and LTO contents of recovered samples.[a]

No.	Ball mill time (h)	ρ_{00} (g cm^{-3})	ρ_{00}/ρ	v (km s^{-1})	p (GPa)	T (K)	Average grain size (nm)	LTO contents (%)
41	4	5.006	0.9	3.2	90.3	1500	…	…
42		2.225	0.4	3.2	90.3	2400	31	51.3
43		1.112	0.2	3.2	90.3	3000	23	79.7
61	6	5.006	0.9	3.2	90.3	1500	…	…
62		2.225	0.4	3.2	90.3	2400	30	59.2
63		1.112	0.2	3.2	90.3	3000	28	100
60 (SSR)	6	…	…	…	…	1473	…	100

[a]ρ is the theoretical density of precursor powder, ρ_{00} is the precursor powder mass to sample container volume, v is the flyer velocity, and No. 60 sample is the synthesized by the SSR method in this study.

The impact velocity (u_{max}) values were calculated according to the Gürney equation,[41]

$$u_{max} = D\left[1 - \frac{1}{\eta}\left(\sqrt{1+2\eta} - 1\right)\right], \tag{1}$$

$$\eta = \frac{16\rho_0 l}{27\rho_M d}, \tag{2}$$

where D is the detonation velocity of the explosive, ρ_0 is the density of explosive, l is the height of the main charge, ρ_M is the flyer density, and d is the flyer thickness.

The equation of state of porous powder was transformed using the Mie–Grüneisen equation of the components and a mixture method.[41–43] In the calculation, the mixed powders were treated as a thin wafer surrounded by copper. At the upper and lower interfaces between the mixed powder thin wafer and surrounding copper, the shock wave reflects and increases the pressure. After multiple reflections, the sample pressure reaches the pressure at the interface of the copper box and the flyer. The shock pressure values were calculated based on the impedance match method.[41,44] Figure 2 shows the impedance matching technique for determining the shock-loading states in the precursor powder at an impact velocity of 3.2 km/s. Note that during above calculation processes, each precursor tablet was treated as a thin wafer surrounded by copper material.[33] The shock temperature in the precursor powder is given as the values of those induced by the first wave in the multiple reflection, owing to that the subsequent reflection waves show little influence on the Hugoniot energy increase. Equation (3)[41] was used to calculate the shock temperature, which is given by

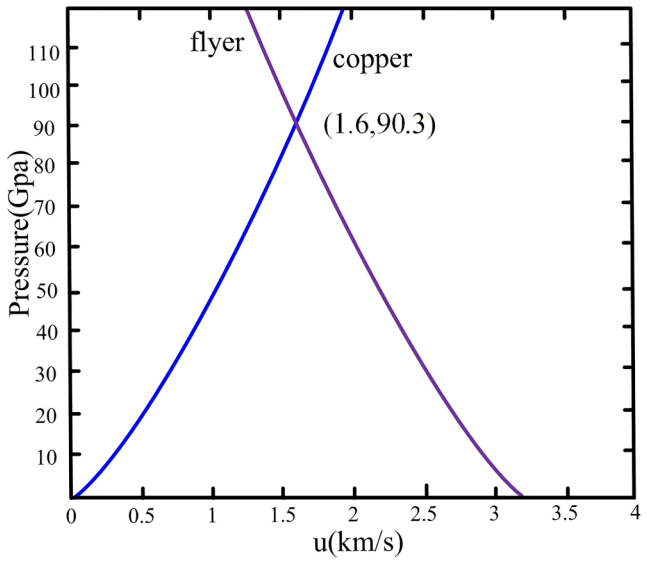

FIG. 2. Illustration of impedance matching technique for determining shock-loading states at an impact velocity of 3.2 km/s.

$$T_1 = T_0 \exp\left[\left(\frac{\gamma_0}{V_0}\right)(V_0 - V)\right] + \frac{(V_0 - V)}{2C_V}P + \frac{\exp\left[\left(-\frac{\gamma_0}{V_0}\right)V\right]}{2C_V} \int_{V_0}^{V} P \times \exp[(\gamma_0/V_0)V]\left[2 - \frac{\gamma_0}{V_0}(V_0 - V)\right]dV, \tag{3}$$

where T_0 is the initial temperature, T_1 is the shock temperature, γ_0 is the Grüneisen coefficient, V_0 and V are initial specific volume and specific volume corresponding to the determined shock pressure P, respectively, and C_v is the specific heat at constant volume. Above calculation results are also listed in Table I for further analysis.

X-ray diffraction (XRD) patterns of the recovered sample were recovered samples and were recorded by operating BRUKER D8 at a working voltage of 40 kV and a working current of 40 mA with Cu Kα radiation. The phase analysis and content of recovered samples were investigated through XRD results. The microstructures and morphology of the samples were characterized by using a Tecnai G^2 F30 transmission electron microscope (TEM) with an accelerating voltage of 300 kV and a HITACHI S4800 scanning electron microscope (SEM), respectively. The UV–vis diffuse reflectance spectra (DRS) were obtained using a UV-3600 spectrophotometer equipped with an integrating sphere assembly with $BaSO_4$ as the reflectance standard

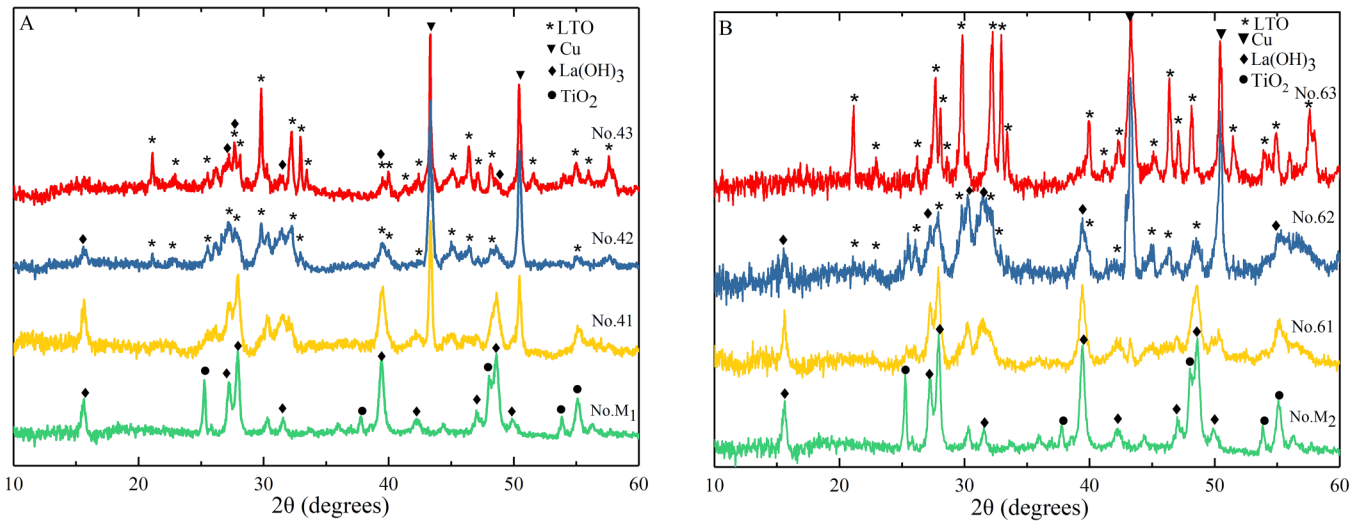

FIG. 3. XRD patterns of (a) the M_1 sample and Nos. 41–43 samples and (b) the M_2 sample and Nos. 61–63 samples.

RESULTS AND DISCUSSION

XRD provides a quick, simple, and effective phase characterization of the recovered samples. Figure 3(a) shows the XRD patterns of the precursor powder with 4-h ball milling treatment (sample M_1) and the recovered samples of Nos. 41–43. The XRD pattern of ball-milled precursor powder presents the characteristic peaks at 15.6°, 25.3°, 27.3°, 27.9°, 39.5°, 48.3°, 48.6°, and 55.3°, which are identified to be the phases of $La(OH)_3$ (formed in the reaction of La_2O_3 and H_2O gas) and TiO_2. This result indicates that LTO can hardly be produced by the ball milling process in our study. The XRD patterns of the No. 41 sample present the XRD phases of $La(OH)_3$, TiO_2, and copper, indicating that LTO cannot be formed under the condition of No. 41 experiment. The XRD patterns of Nos. 42 and 43 samples show the characteristic peaks of $La(OH)_3$, TiO_2, LTO, and copper, indicating the presence of shock-synthesized LTO in the recovered sample. The specific LTO peak positions from XRD results are also listed in Table II for further discussion. Note that the copper fragments in the sample are from the copper inner wall of the sample chamber. Furthermore, the XRD patterns also reveal that the condition of low relative density intense characteristic peaks of the LTO phase, implying the increase of LTO content in the recovered sample with condition of low relative density. Through the Scherrer equation, the average grain sizes of Nos. 42 and 43 samples are calculated to be of 38 and 21 nm, indicating that the recovered LTO powder is nanocrystalline, which is in accordance with previous studies and the formation process of shock synthesis in microseconds.

To further enhance the activity of the precursor, the same La_2O_3 and TiO_2 powders were mixed through a 6-h ball milling treatment. Figure 3(b) shows the XRD patterns of the precursor powder (the M_2 sample) and Nos. 61–63 samples. The XRD pattern of the M_2 sample presents XRD peaks appearing at 15.6°, 25.3°, 27.3°, 27.9°, 39.5°, 48.1°, 48.6°, and 55.3°, which is same with that of the M_1 sample, showing the presence of only $La(OH)_3$ and TiO_2 phases. XRD patterns of Nos. 61–63 experiments show the presence of LTO characteristic peaks whose intensity increases with the decrease of relative density of precursor powder before shock compression. No. 63 sample consists of only copper and LTO,

TABLE II. Theoretical and experimental d-spacing values from previous studies, and the obtained d-spacing values of XRD and SAED data in our study.

hkl	Relative intensity/I (%)	LTO (PDF No. 27-1182)	No. 43	No. 63
(210)	50	4.201	4.207	4.209
(002)	20	3.860	3.891	3.890
(310)	20	3.390	3.313	3.352
(400)	80	3.217	3.221	3.225
(202)	20	3.110		3.178
($\bar{2}$12)	100	2.989	2.997	2.999
(020)	80	2.775	2.778	2.780
(212)	80	2.714	2.717	2.718
(022)	20	2.251	2.254	2.256
(600)	10	2.140		2.149
(412)	50	2.131	2.136	2.135
(420)	50	2.099		2.091
(222)	20	2.069		2.075
($\bar{1}$04)	50	1.950	1.956	1.958
($\bar{4}$22)	20	1.924	1.928	1.929
(403)	50	1.880	1.889	1.889
($\bar{4}$04)	20	1.772		1.774
(032)	20	1.668	1.669	1.672
(132)	20	1.640		1.642

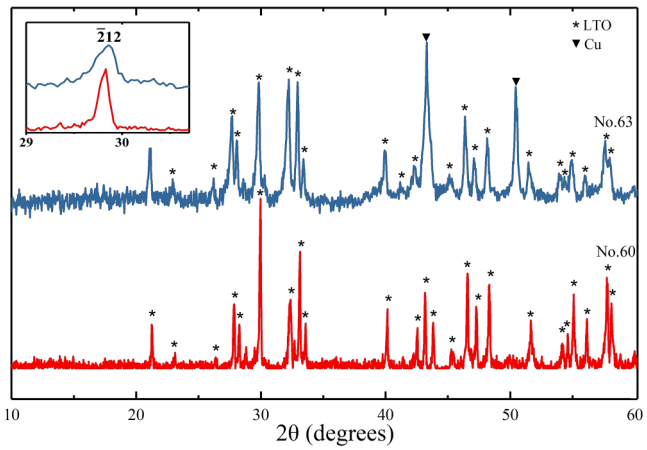

FIG. 4. XRD patterns of Nos. 60 and 63 samples.

indicating that the LTO yield under this condition is up to 100%. Through, the Scherrer equation, the average grain sizes of Nos. 62 and 63 samples are calculated to be of 30 and 28 nm, indicating that the recovered LTO powder is nanocrystalline.

The content of LTO is further calculated based on the adiabatic approximation method as follows:

$$W_X = \frac{I_X}{K_A^X \sum_{i=1}^{N} \frac{I_i}{K_A^i}}, \tag{4}$$

$$K_A^X = \frac{K_{Al_2O_3}^X}{K_{Al_2O_3}^A}, \tag{5}$$

where A is the internal standard phase, W_X indicates the phase X content, I_X is the peak intensity of phase X, $K_{Al_2O_3}^X$ and $K_{Al_2O_3}^A$ are the XRD-peak intensity ratios of corresponding phases to α-Al_2O_3, and I_i is the peak intensity of phase i. The calculation results are listed in Table I, further confirming that the decease of relative density of the precursor and increase of the ball milling period improve the LTO content of the recovered sample. With respect to Nos. 41–43 samples, as the relative density decreases from 90% to 20%, the LTO yield increases from 0% to 79.7%. When the ball milling treatment is up to 6 h, the LTO yield of the recovered samples under corresponding relative density further increase from 51.3% to 59.2% (40% density) and from 79.7% to 100% (20% density), respectively. During the shock compression process, low

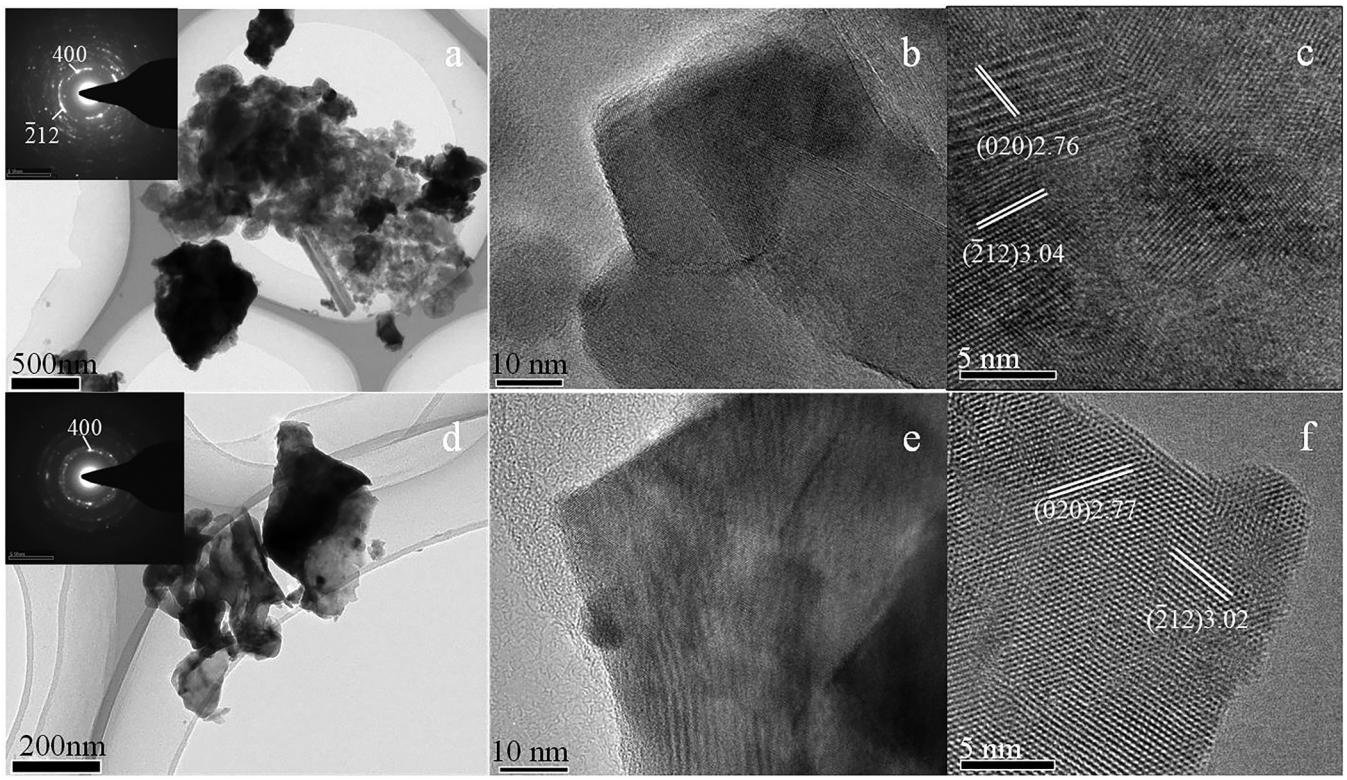

FIG. 5. High-resolution TEM imagines of shock-synthesized LTO obtained from (a)–(c) No. 43 sample and (d)–(f) No. 63 sample. The insets in (a) and (d) present the typical SAED patterns of Nos. 43 and 63 samples.

TABLE III. Interplanar spacings calculated by SAED patterns for shock-synthesized LTO obtained from No. 43 sample and No. 63 sample.

	d-spacing values [d(hkl)](Å)		
hkl	LTO (PDF No. 27-1182)	No. 43	No.63
$\bar{2}10$	4.20	4.15	
400	3.22	3.18	3.23
$\bar{2}12$	2.99	3.04	3.02
020	2.77	2.76	2.77
022	2.25	2.25	2.27
$\bar{1}04$	1.95	1.94	1.94

relative density enhances the adiabatic compression, leading to higher shock temperature, which is conducive to the chemical reaction to form LTO.

Figure 4 presents the XRD patterns of Nos. 60 and 63 samples for the comparison of two LTO samples synthesized by shock synthesis and SSR methods. The XRD results reveal that the characteristic peaks in both patterns are in good accordance with that of previous LTO, further confirming the shock-induced synthesis of LTO. Moreover, the full width at half maximum (FWHM) of XRD peaks of No. 63 sample is larger than that of the corresponding peaks of No. 60 sample, suggesting that the crystal size of shock-synthesized LTO is smaller than that of LTO obtained by the SSR method.

Typical TEM images of LTO Nos. 43 and 63 samples [Figs. 5(a), 5(b), 5(d), and 5(e)] show the presence of irregular polyhedral nanoparticles composed of multiple crystal sizes of approximately 15–50 nm. The corresponding high-resolution TEM (HRTEM) further reveals the high crystallinity of nano-LTO crystals and their d-spacing values of 2.76, 3.04, and 3.18 Å, which are in accordance with the d(020), d(−212), and d(400) of LTO (PDF No. 27-1182). Furthermore, the insets in Figs. 5(a) and 5(d) present the SAED patterns of the recovered samples, showing several ring-like diffraction patterns with dispersed bright spots, which indicate the presence of highly crystalline multiple crystals in the recovered samples. The d-spacing values of Nos. 43 and 63 samples were also analyzed through the SAED pattern [the inset of Figs. 5(a) and 5(d)] and are listed in Table III with d-spacing values of LTO obtained from a previous study (PDF No. 27-1182) for comparison. The results show that the d-spacing values of shock-synthesized LTO are in good agreement with the XRD results and the previous synthesized LTO using other methods.

Typical SEM images (Fig. 6) of the LTO powder prepared by the shock method reveal the practical morphology of LTO powders with irregular polyhedral shape, and the particles stick to each other. Based on the statistics of SEM examinations, the sample particles are in a size of 50 nm, which is in good agreement with XRD and TEM results. Besides, Figs. 6(c) and 6(f) reveal the rapidly melted and solidified morphology at the boundaries of particles in Nos. 43 and 63 samples, implying the high temperature during shock treatment. In addition, the spherical particle in Fig. 6(f) further confirms the melting process during shock treatment, which is supposed to be conducive to the LTO formation. Consequently, the LTO formation state (Fig. 6) is in good

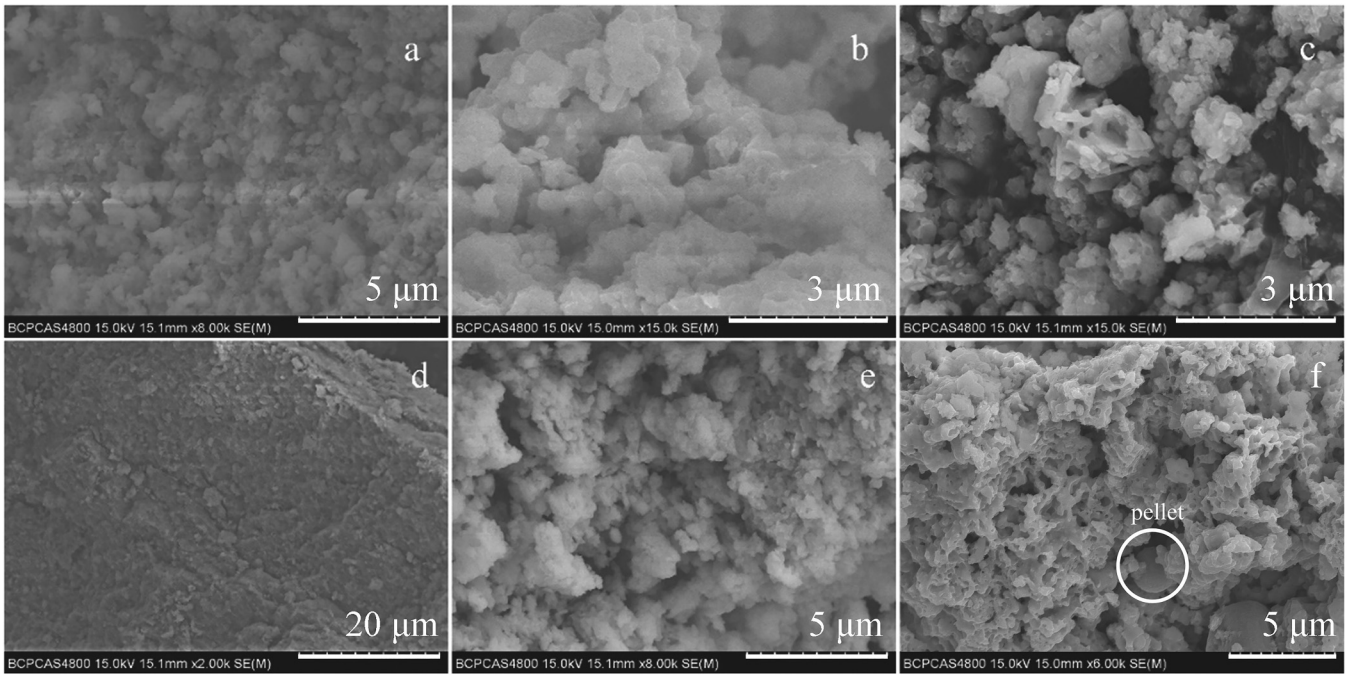

FIG. 6. Typical SEM images of (a) No. 41 sample, (b) No. 42 sample, (c) No. 43 sample, (d) No. 61 sample, (e) No. 62 sample, and (f) No. 63 sample.

agreement with the calculation results. Under this condition, La_2O_3 and TiO_2 with high activity react to form LTO with high yield. The low relative density increases the shock temperature to induce the melt of precursor powder and liquid phase chemical reaction, which increase the LTO yield.

The UV–vis spectra of Nos. 60 and 63 samples are shown in Fig. 7, suggesting that the spectrum of No. 63 sample features red-shifts to the absorption edge of about 640 nm compared with that of No. 60 sample. Furthermore, No. 63 samples exhibit enhanced adsorption in the whole visible-light region. It may be caused by the defects such as oxygen vacancy and dislocation formed under shock wave action.[45]

The formation mechanism of shock-synthesized LTO is carefully discussed below. La_2O_3 powder and TiO_2 powder were mixed and activated using ball milling. Then, the mixed precursor was filled into the sample chamber and impacted by the shock-driven flyer. Shock compression action, an adiabatic compression process, induces a rapid increase in the temperature and pressure to 10^3 K and 10^1 GPa, respectively. This extreme condition leads to the chemical reaction of activated precursor to form LTO powder in microseconds. Considering such a narrow reaction window, the shock temperature decreases dramatically in microseconds, which inhibit the growth of the formed LTO nanocrystal, leading to the presence of nanograins with an average size of 20–30 nm in the recovered samples.

During the shock compression process, the initial relative density of the precursor powder influences greatly the shock temperature. When the relative density of the precursor powder is high (90%), the calculated shock temperature is 1500 K lower than the melting points of La_2O_3 (2588 K) and TiO_2 (2113 K). Consequently, the yield of LTO is low, considering the transform efficiency of the solid phase reaction in such narrow reaction windows. As the relative density of precursor powder decreases, the shock temperature increases to induce a liquid–solid reaction of precursor powders with higher activity, leading to the increase of LTO yield. When the relative density is 20%, the calculated shock temperature is 3000 K, which further enhances the melting degree, fusion degree, and chemical activity of precursor powder, leading to the synthesis of LTO with yield over 90%. Moreover, ball milling treatment refines the precursor particles and generates defects in the powder, leading to the increase of chemical activation. A longer ball milling treatment leads to higher activity of precursor powder by forming more defects in the particles. Thus, the long period ball milling treatment can further increase the LTO yield under conditions of same relative density during shock treatment. Based on our study, when the relative density is 20% and the ball milling period is 6 h (No. 63 sample), the precursor powder fully reacts to form LTO with a yield of 100%.

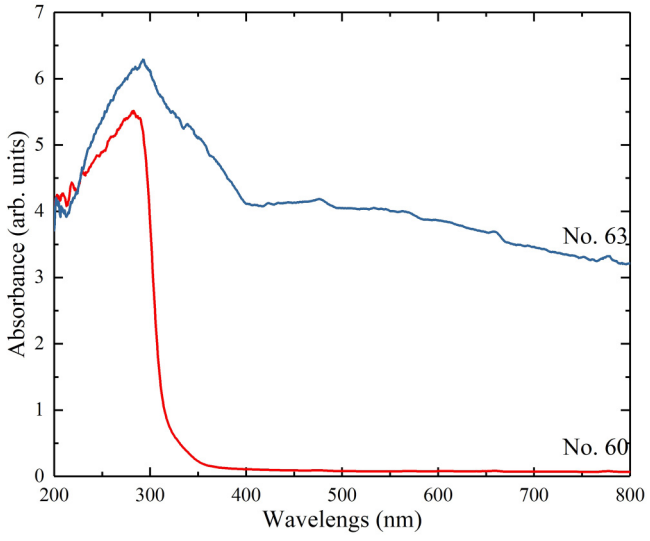

FIG. 7. The UV–vis spectra of Nos. 60 and 63 samples.

Our study implies that the shock synthesis method is a highly potential one to synthesize bimetal oxide nanocrystalline powder. Furthermore, shock treatment is an ideal approach to obtain doping powder and shock-activated powder, implying the potential one-step synthesis of doped perovskite powder for further step investigations.

CONCLUSION

LTO was synthesized successfully by the shock compression method. The average crystal size of LTO was approximately 30 nm. Under the shock treatment, the temperature and pressure of the precursor activated by the ball milling treatment increase rapidly in microseconds, inducing the chemical reaction to form nano-LTO crystals. Our study demonstrates that the shock temperature and ball milling activation were two critical factors to synthesize LTO with the shock synthesis method. The low relative density of precursor powder induces high shock temperature and longer ball milling time further increases the chemical reaction. The 6-h ball-milled precursor powder with 20% relative density forms LTO with a yield of 100% under shock compression. This study proves a novel approach to synthesize perovskite materials.

SUPPLEMENTARY MATERIAL

See the supplementary material for the size of the experiment setup.

ACKNOWLEDGMENTS

This research was supported by the project of State Key Laboratory of Explosion Science and Technology, Beijing Institute of Technology (Grant No. ZDKT18-01).

DATA AVAILABILITY

The data that support the findings of this study are available within the article.

REFERENCES

[1]M. Wu, S. Yu, L. He, and L. Yang, Mater. Lett. **174**, 201 (2016).
[2]J. Li, S. Xiong, Y. Liu, Z. Ju, and Y. Qian, Am. Chem. Soc. **5**, 981 (2013).
[3]H. Tang, M. Jiang, Y. Zhang, X. Lai, C. Cui, H. Xiao, S. Jiang, E. Ren, Q. Qin, and R. Guo, Electrochim. Acta **354**, 136760 (2020).

[4]R. Jose, V. Thavasi, and S. Ramakrishna, Am. Ceram. Soc. **92**, 289 (2010).
[5]Y. Yin, Y. Shen, P. Zhou, R. Lu, A. Li, S. Zhao, W. Liu, D. Wei, and K. Wei, Appl. Surf. Sci. **509**, 145335 (2020).
[6]Z. Wang, F. Wei, Y. Sun, J. Qi, Y. He, and Q. Meng, Ceram. Int. **45**, 12558 (2019).
[7]J. Feng, B. Xiao, C. L. Wan, Z. X. Qu, Z. C. Huang, J. C. Chen, R. Zhou, and W. Pan, Acta Mater. **59**, 1742 (2011).
[8]N. Zhang, Q. J. Li, S. G. Huang, Y. Yu, J. Zheng, C. Cheng, and C. C. Wang, J. Alloys Compd. **652**, 1 (2015).
[9]W. J. Weber and R. C. Ewing, Science **289**, 2051 (2000).
[10]X. G. Chen and H. S. Zhang, Adv. Mater. Res. **624**, 22 (2012).
[11]E. V. Dudnik, S. N. Lakiza, N. I. Hrechanyuk, A. K. Ruban, V. P. Red'ko, M. S. Hlabay, and A. B. Myloserdov, Powder Metall. Met. Ceram. **57**, 301 (2018).
[12]Z. Fulan, Z. Jiwu, S. Lanqian, X. Yihong, C. Guohui, Z. Yong, and L. Jinlin, Sci. Rep. **7**, 1 (2017).
[13]P. Duan, C. Han, Y. Zheng, G. Cai, F. Zhong, and Y. Xiao, J. Alloys Compd. **831**, 154866 (2020).
[14]A. V. Shlyakhtina, K. S. Pigalskiy, D. A. Belov, N. V. Lyskov, E. P. Kharitonova, I. V. Kolbanev, A. B. Borunova, O. K. Karyagina, E. M. Sadovskaya, V. A. Sadykov, and N. F. Eremeev, Dalton Trans. **47**, 2376 (2018).
[15]R. C. Ewing, W. J. Weber, and J. Lian, J. Appl. Phys. **95**, 5949 (2004).
[16]Y. Ku, L. C. Wang, and C. M. Ma, Chem. Eng. Technol. **30**, 895 (2007).
[17]Y. Abe and R. M. Laine, J. Am. Ceram. Soc. **103**, 4832 (2020).
[18]Y. Cao, P. Tang, Y. Han, and W. Qiu, J. Alloys Compd. **842**, 155581 (2020).
[19]W.-M. Hou and Y. Ku, J. Alloys Compd. **509**, 5913 (2011).
[20]J. Zhang, W. Hu, S. Cao, and L. Piao, Nano Res. **13**, 2313 (2020).
[21]H. G. Kim, D. W. Hwang, S. W. Bae, J. H. Jung, and J. S. Lee, Catal. Lett. **91**, 193 (2003).
[22]M. Han, Z. Ma, W. Zhang, and H. Wang, J. Sol-Gel Sci. Technol. **96**, 480 (2020).
[23]D. Chen and R. Xu, Mater. Res. Bull. **33**, 409 (1998).
[24]A. V. Prasadarao, U. Selvaraj, and S. Komarneni, J. Mater. Res. **7**, 2859 (1992).
[25]Z. Huang, J. Liu, and L. Huang, NPG Asia Mater. **12**, 11 (2020).
[26]A. Arab, Y. Guo, Q. Zhou, and P. Chen, Entropy **21**, 880 (2019).
[27]G. Hillel, L. Meshi, S. Kalabukhov, N. Frage, and E. B. Zaretsky, Acta Mater. **187**, 176 (2020).
[28]X. Gao, P. Chen, and J. Liu, Mater. Lett. **65**, 685 (2011).
[29]H. Yin, P. Chen, C. Xu, X. Gao, Q. Zhou, Y. Zhao, and L. Qu, Carbon **94**, 928 (2015).
[30]O. Tschauner, S. N. Luo, Y. J. Chen, A. McDowell, J. Knight, and S. M. Clark, High Press. Res. **33**, 202 (2013).
[31]J. Liu and G. Lu, Mater. Res. Bull. **31**, 1049 (1996).
[32]S. S. Batasanov, L. I. Kopaneva, and G. V. Dorogova, Russ. J. Inorg. Chem. **28**, 1222 (1983).
[33]Z. Tan, P. Chen, Q. Zhou, J. Liu, X. Mei, B. Wang, and N. Cui, J. Phys.: Condens. Matter **30**, 1 (2018).
[34]B. Turner-Adomatis and N. Thadhani, Mater. Sci. Eng. A **256**, 289 (1998).
[35]E. K. Beauchamp and M. J. Carr, J. Am. Ceram. Soc. **73**, 49 (2010).
[36]Y. Sekine, K. Kodama, T. Kobayashi, S. Obata, Y. Chang, N. O. Ogawa, Y. Takano, N. Ohkouchi, K. Saiki, and T. Sekine, Meteorit. Planet. Sci. **53**, 1267 (2018).
[37]P. W. Chen, Y. S. Ding, Q. Chen, F. L. Huang, and S. R. Yun, Diamond Relat. Mater. **9**, 1722 (2000).
[38]V. V. Sobolev, Y. N. Taran, and S. I. Gubenko, J. Phys. IV **7**, C3-73 (1997).
[39]P. Chen, F. Huang, and S. Yun, Carbon **41**, 2093 (2003).
[40]X. Gao, J. Liu, and P. Chen, Mater. Res. Bull. **44**, 1842 (2009).
[41]M. A. Meyers, *Dynamic Behavior of Materials* (Wiley, New York, 1994).
[42]M. A. Meyers, *LASL Shock Hugoniot Data* (Wiley, New York, 1994).
[43]S. P. Marsh, *LASL Shock Hugoniot Data* (University of California Press, Berkeley, CA, 1980).
[44]T. J. Ahrens and M. L. Johnson, *Shockwave Date for Materials* (1995).
[45]J. Soria, J. Sanz, I. Sobrados, J. M. Coronado, F. Fresno, and M. D. Hernández-Alonso, Catal. Today **129**, 240 (2007).